HHS Public Access

Author manuscript

Curr Biol. Author manuscript; available in PMC 2021 June 22.

Published in final edited form as:

Curr Biol. 2020 June 22; 30(12): 2225–2237.e5. doi:10.1016/j.cub.2020.04.025.

Sites of Circadian Clock Neuron Plasticity Mediate Sensory Integration and Entrainment

Maria P Fernandez[1,4,*], **Hannah L. Pettibone**[1,2], **Joseph T. Bogart**[1], **Casey J Roell**[2], **Charles E. Davey**[2], **Ausra Pranevicius**[4], **Khang V. Huynh**[2], **Sara M. Lennox**[2], **Boyan S. Kostadinov**[3], **Orie T. Shafer**[1,2,*,#]

[1]-Advanced Science Research Center, The Graduate Center, City University of New York. New York City, NY 10031, U.S.A.

[2]-Department of Molecular, Cellular, and Developmental Biology, University of Michigan. Ann Arbor, MI 48109, U.S.A.

[3]-Mathematics Department, NYC College of Technology, City University of New York. Brooklyn, NY 11201, U.S.A.

[4]-Department of Neuroscience and Behavior, Barnard College of Columbia University. New York City, NY 10027, U.S.A.

Summary

Networks of circadian timekeeping in the brain display marked daily changes in neuronal morphology. In *Drosophila melanogaster*, the striking daily structural remodeling of the dorsal medial termini of the small ventral lateral neurons has long been hypothesized to mediate endogenous circadian timekeeping. To test this model, we have specifically abrogated these sites of daily neuronal remodeling through the reprogramming of neural development and assessed the effects on circadian timekeeping and clock outputs. Remarkably, the loss of these sites has no measurable effects on endogenous circadian timekeeping or on any of the major output functions of the small ventral lateral neurons. Rather, their loss reduces sites of glutamatergic sensory neurotransmission that normally encodes naturalistic time-cues from the environment. These

[*]Correspondence should be addressed to OT Shafer, Neuroscience Initiative, Advanced Science Research Center, at oshafer@gc.cuny.edu or Maria de la Paz Fernandez, Department of Neuroscience and Behavior, Barnard College of Columbia University, at mfernand@barnard.edu.

[#]Lead Contact.

Author Contributions

Maria P Fernandez: Conceptualization, Formal Analysis, Funding acquisition, Investigation, Project administration, Supervision, Writing – original draft, and Writing – review & editing. Hannah L. Pettibone: Formal Analysis, Investigation, Validation, and Writing – review & editing Joseph T. Bogart: Formal Analysis, Investigation, Validation, and Writing – review & editing. Casey J Roell: Formal Analysis and Methodology. Charles E. Davey: Investigation and Data curation. Ausra Pranevicius: Investigation, Formal Analysis. Khang V. Huynh: Investigation and Formal Analysis. Sara M. Lennox: Investigation and Formal Analysis. Boyan S. Kostadinov: Conceptualization, Methodology, Software, Visualization and Writing – review & editing. Orie T. Shafer: Conceptualization, Funding acquisition, Investigation, Project administration, Supervision, Validation, Writing – original draft, and Writing – review & editing.

Declaration of Interests:

The authors declare no competing interests.

results support an alternative model: structural plasticity in critical clock neurons is the basis for proper integration of light and temperature and gates sensory inputs into circadian clock neuron networks.

eTOC Blurb

Fernandez *et al.* show that sites of daily structural plasticity in key clock neurons are not required for circadian timekeeping. Rather, these sites are required for normal entrainment to naturalistic environmental temperature cycles. These results suggest that changes in neural structure alter the clock network's sensitivity to sensory input.

Introduction

The circadian system influences the daily timing of activity through two processes, endogenous circadian timekeeping and the daily resetting of circadian rhythms to local time (i.e., entrainment) [1]. The importance of these two processes for health are made clear by a growing body of evidence that modern environments result in weak and unstable circadian entrainment, leading to a loss of sleep, increased cancer risk, and metabolic derangement [2]. The master circadian clock resides in small islands of brain tissue [3] wherein connections among diverse neuron types ensure a robustness in circadian timekeeping that is lacking in peripheral tissues [4]. Such circadian timekeeping networks require sensory inputs to entrain to daily environmental rhythms [5]. Understanding the network properties of circadian timekeeping and entrainment is a central challenge in chronobiology.

Critical neurons within timekeeping networks in both insect and mammalian brains undergo daily changes in cellular morphology (reviewed by [6, 7]). In *Drosophila* the small ventrolateral neurons (s-LN_vs) undergo daily structural remodeling, displaying significantly more highly branched dorsomedial projections in the early day relative to the early night [8], a rhythm driven by daily changes in outgrowth and de-fasciculation [9–11]. Daily s-LN_v remodeling is driven by daily rhythms in clock-controlled gene expression [9, 10, 12, 13] and is therefore considered an output of the molecular clock within these neurons. The s-LN_vs are critical for circadian timekeeping and properly timed behavioral outputs and produce the neuropeptide Pigment Dispersing Factor (PDF), which is likewise required for robust circadian timekeeping [14, 15]. The dorsal termini of the s-LN_vs contain both synaptic and dense core vesicles and their daily structural changes occur among the neurites of s-LN_v output targets [11, 16]. For these reasons, the dorsal termini of the s-LN_vs have long been considered the major sites of s-LN_v axonal output [14, 16] and their daily structural plasticity is generally assumed to be a mechanism of circadian clock output [6].

Within the hypothalamic suprachiasmatic nuclei (SCN), neurons expressing the neuropeptide vasoactive intestinal poly-peptide (VIP) support circadian rhythms in a manner remarkably similar to PDF expressing s-LN_vs in *Drosophila*. The loss of VIP signaling results in a syndrome of circadian phenotypes that are highly reminiscent of those accompanying the loss of PDF in the fly [15, 17–21]. The VIP neurons of the SCN undergo daily changes in morphology, displaying increased glial coverage of somata and dendrites during the day [22]. The morphological changes exhibited by SCN VIP neurons are

accompanied by daytime increases in synaptic inputs, including glutamatergic inputs from the eye [23]. Furthermore, retino-recipient Calbindin-D28K expressing neurons in the hamster SCN display more elaborate arborizations in the early subjective night compared to other times [24]. Thus, the plasticity in the mammalian SCN may serve to mediate the integration of sensory input [23], however the large numbers and heterogeneity of SCN neurons make a mechanistic examination of the function of such plasticity difficult to address experimentally.

An increasing number of studies have reported manipulations of the s-LN_v dorsal termini that are accompanied by significant effects on circadian timekeeping [9, 10, 12, 13, 25]. For example, the overexpression of the clock-controlled transcription factor Mef2 results in both constitutively open/complex termini and in a significant reduction in the percentage of flies able to maintain endogenous circadian rhythms in activity [10]. Likewise, the overexpression of the Rho1 GTPase in LN_v neurons results in both constitutively simple/closed termini and a significant weakening of locomotor rhythms [9]. However, manipulations that cause significant morphological changes in the dorsal termini but nevertheless fail to alter free-running circadian rhythms or clock outputs have also been reported [9, 10, 12, 25]. Thus, the functional significance of daily s-LN_v structural plasticity has not been unequivocally established.

Here we take advantage of the genetic malleability and relative simplicity of the *Drosophila* clock neuron network to examine the functional significance of sites of circadian neuronal remodeling in the s-LN_vs. By manipulating a well characterized mechanism of neuronal path finding, we have specifically prevented the development of the s-LN_v dorsal termini and comprehensively assessed the effects of their loss on endogenous circadian timekeeping and phasing of clock output. We find that the PDF-mediated circadian timekeeping and output functions of the s-LN_vs remain unchanged in the absence of these plastic terminal arborizations. Rather, we find that these termini mediate sensory inputs and the proper integration of time-cues from the environment. These results provide clear evidence that the sites of daily structural remodeling mediate sensory input and entrainment within the circadian clock neuron network and suggest that daily structural plasticity likely shapes the responses of circadian clock neurons to temporal cues from the environment.

Results

The expression of Unc5 specifically prevents the formation of the s-LN_v dorsal projection termini.

Previous work investigating the relationship between s-LN_v structural plasticity and circadian timekeeping employed genetic manipulations that clamped the dorsal termini in constitutively open or closed configurations, typically through the up- or down-regulation of transcription factors or cell signaling pathways (e.g. [9, 10]). Most such manipulations have resulted in significant deficits in circadian sleep/activity rhythms. However, several manipulations that produce defects in s-LN_v arbor morphology and/or plasticity have failed to produce circadian output phenotypes (e.g., [10, 12]), suggesting that dorsal termini manipulations that have produced circadian phenotypes may have acted via effects that were independent of the terminal arbor phenotypes they produced. Thus, the functional

significance of such plasticity remains an open question. For this reason, we sought to disrupt the formation of these termini developmentally to test the prediction that the absence of the sites of s-LN_v plasticity would produce timekeeping phenotypes reminiscent of the loss of s-LN_vs or their major circadian peptide output PDF.

The formation of s-LN_v dorsal termini requires a turn toward the midline of the dorsal protocerebrum and the de-fasciculation of s-LN_v dorsal projections into radiating processes (Figs. 1A and 1C; [26, 27]). The over-expression of the repulsive netrin receptor Unc5 in all PDF expressing neurons abrogated the terminal ramification of the s-LN_v dorsal projections (Figure 1 and S1A), most likely by preventing normal developmental outgrowth of these termini toward the midline where netrin is secreted during embryonic development [28]. Unc5 overexpressing s-LN_vs displayed a severely simplified dorsal projection that lacked the dorsal medial termini (Figure 1A–G), a phenotype reflected by significant reductions in both the length of the dorsal projections and the brain volume they innervate (Figs. 1D–E). Unc5 overexpression was also accompanied by modest de-fasciculation of the ascending dorsal projection of the s-LN_vs (arrowhead in Figure 1A, right panel, and S1C). No evidence of residual plasticity was found in the s-LN_v arbors of Unc5 expressing flies (Fig 1D–E). Unc5 overexpression had no obvious effects on the anatomy of the large LN_vs (Figs. 1A, and S1B). We conclude that the overexpression of Unc5 specifically prevents the formation of the plastic s-LN_v dorsal termini.

PDF-mediated output functions of the s-LN_vs do not require their dorsal termini.

If the plastic dorsal termini of the s-LN_vs are critical for circadian timekeeping and output signals, the loss of these termini should behaviorally phenocopy the ablation of these cells or the genetic loss of PDF, their major circadian output transmitter [15]. The loss of the LN_vs and PDF both result in a syndrome of timekeeping phenotypes that includes the loss of morning anticipation, an advance in the daily evening peak of activity under light/dark (LD) cycles, and a significant weakening of the endogenous circadian rhythm under constant darkness and temperature (DD) accompanied by a decrease in free-running period [15] (Figs. 2A, B, E and 3A). Under a 12h:12h LD cycle, the overexpression of Unc5 in PDF expressing neurons had no measurable effects on the anticipation of LD transitions or on the entrained phase of evening peak activity, with *Pdf-Gal4/UAS-Unc5* flies exhibiting normal daily profiles of locomotion that displayed the normal anticipation of light transitions (Figs. 2C–E, S2, and S3). The s-LN_vs exert control over much of the circadian clock neuron network through PDF mediated resetting signals [29–31]. When the molecular clocks within the s-LN_vs are slowed down by the expression of the mutant clock kinase $Doubletime^{LONG}$ (Dbt^{LONG}), the daily evening peak of activity is delayed (Figure S4A), reflecting a resetting of the so called “evening cells” of the clock neuron network by PDF [30, 31]. Remarkably the s-LN_vs were still able to set the evening peak of activity in the absence of their dorsal termini (Figure S4A).

The s-LN_vs are the most dominant circadian pacemakers within the clock neuron network under conditions of constant darkness and temperature (DD) [32]. The loss of PDF peptide or genetic ablation of the LN_vs dramatically weakens the endogenous circadian rhythm and produces a shortening of its free-running period under DD [15]. When the speed of the

molecular clock is changed within s-LN_vs, PDF released from these neurons resets the molecular clocks within other clock neurons and modulates the systemic timekeeping [29–32]. If the plastic dorsal termini of the s-LN_vs mediate these circadian output functions, we would expect to see clear timekeeping phenotypes under DD. The loss of the dorsal termini in Unc5 expressing LN_vs was not accompanied by changes in the proportion of flies displaying circadian rhythms in locomotor activity following entrainment to LD cycles, nor did it produce a shortening of its free-running period (Figs. 3A and 3D, S4B, and Table S1). The expression of the mutant clock kinase Dbt^{LONG} only in the PDF expressing LN_vs coherently sets the period of free-running sleep/activity rhythms to approximately 27 hours [30, 31]. Remarkably, the co-expression of Unc5 with Dbt^{LONG} in the LN_vs did not prevent these neurons from lengthening the free-running period of locomotor rhythms nor from delaying the evening peak of activity on the first day of free-run ((Figure 3A–C, and S4B). Thus, the ability of the s-LN_vs to control the clock neuron network was not affected by the absence of their normal sites of daily remodeling. We conclude that the normal sites of structural plasticity in the dorsal projections of the s-LN_vs are not required for the established PDF-dependent output functions of these neurons.

The loss of s-LN_v dorsal termini causes deficits in the entrainment of locomotor rhythms to naturalistic ramping temperature cycles.

The dorsal termini of the s-LN_vs rest in close apposition to the neurites of the $DN1_p$ class of clock neurons, which are established targets of LN_v output [33, 34] and serve as major conduits of circadian output signals in the fly brain [35]. Serial electron micrograph (SEM) reconstructions of the s-LN_v termini revealed the presence not only of output (i.e., pre-synaptic) synapses, but also post-synaptic structures, indicating that the dorsal termini serve as sites of both input and output [16]. The $DN1_p$s provide glutamate-mediated inhibitory inputs onto the s-LN_vs [36]. Thus, the s-LN_vs and $DN1_p$s form bidirectional connections. The sites of PDF release from the dorsal termini of the s-LN_vs appear to be extrasynaptic: PDF-containing dense core vesicles dock in regions of the dorsal projections that are not directly opposed by post-synaptic compartments [16], suggesting that PDF released from the dorsal termini may normally act at a distance. The dorsal projections of the s-LN_vs typically extend through the medial and lateral neurites of the $DN1_p$s (Figure 4A–C and G–I). In contrast, Unc5 expressing dorsal projections do not extend along these regions of the $DN1_p$s (Figure 4D–F and J–L), whose major projections remain unchanged. Thus, the normal sites of communication within brain region innervated by the lateral and medial extensions of the $DN1_p$s are missing for Unc5 expressing s-LN_vs. However, truncated s-LN_vs continue to display expression of dendritic markers (Figure S7G), suggesting that they are likely capable of receiving some presynaptic inputs via the reduced regions of apposition.

The $DN1_p$s sensitively monitor environmental temperature [37], their synaptic outputs are required for the normal entrainment of sleep/activity cycles to low amplitude step-function temperature cycles [38] and to gradually and constantly ramping temperature cycles [37], and their molecular clocks are entrained by peripheral thermoreceptors [39, 40]. The organization of activity and sleep under such constantly changing temperature cycles is likely mediated by the inhibition of the s-LN_vs by the $DN1_p$s [36, 37]. We hypothesized that the plastic dorsal termini might be required for the normal entrainment to gradually ramping

temperature cycles. We therefore predicted that the abrogation of the s-LN_v dorsal termini would lead to changes in the organization of sleep/activity rhythms under such entrainment conditions.

Under a temperature oscillation that consisted of constant heating from 20 to 28°C for 12 hours followed by constant cooling from 28 to 20°C for 12 hours, *Pdf-Gal4/UAS-Unc5* flies differed significantly from their parental controls with regard to the daily pattern of activity. As previously described for wild type flies [37, 41], the control *Pdf-Gal4/+* and *UAS-Unc5/+* flies displayed a rather small increase in activity at the onset of heating followed by gradual increases in locomotion throughout most of the heating phase, followed by a precipitous drop in activity at onset of cooling (Figure 5A–B). In contrast, *Pdf-Gal4/UAS-Unc5* flies displayed activity rhythms of significantly lower amplitude and did not begin their major daily increase in locomotion until the end of the heating phase, (Figure 5A–B). We quantified the heating index (5C), which is based on the correlation between rising temperatures and locomotor activity [37], which revealed significant differences between *Pdf-Gal4/UAS-Unc5* flies and their parental controls. In contrast to flies entrained to LD cycles (Figure 3), analysis of free running rhythms after temperature ramp entrainment revealed that *Pdf-Gal4/UAS-Unc5* exhibit weaker rhythms as measured by a reduction in the percentage of rhythmic flies (Fig 5D) and a reduction in rhythmic power (Fig 5E). Free-running period was not significantly different from the Gal4 heterozygote control (Figure 5F and Table S1). This differential timekeeping deficit following ramping temperature ramps was reminiscent of flies lacking peripheral temperature inputs [37] and is consistent with weakened entrainment under ramping temperature cycles but not LD cycles.

Quantification of PERIOD expression rhythms in the s-LN_vs under temperature ramp cycles revealed a clear reduction in the amplitude and a change in the phase of diurnal PERIOD rhythms in the s-LN_vs of Unc5 expressing flies (Figure 5 G–H). These results support the conclusion that the absence of s-LN_v dorsal termini is accompanied by an inability to properly entrain the s-LN_vs to constantly changing temperature cycles, likely due, at least in part, to the inability to properly integrate input from thermoreceptors via the $DN1_p$s. However, it is important to note the existence of some residual entrainment in these flies. Though the loss of the s-LN_v dorsal termini caused a significant reduction in the amplitude and timing of daily activity and in the daily rhythm in PER expression in these cells, our experimental flies did nevertheless maintain daily increases in activity near the end of the heating phase. We note that the $DN1_p$s also inhibit evening oscillators (LN_ds) [36], a connection that, along with any remaining connections to the s-LN_vs, may underlie the residual, abnormal entrainment seen in our flies.

Neural activity directly shapes daily changes in dorsal projection structure and temperature changes are predicted to modulate s-LN_v neural activity [36, 37]. If the s-LN_vs receive daily inhibitory inputs from thermo-receptive neurons, we would expect to see daily structural remodeling of the s-LN_v dorsal termini under ramping temperature cycles. We therefore compared arbor volume at ZTs 02 and 14 under such cycles. Indeed, the dorsal termini undergo daily changes in the volume of arbor spread under ramping temperature cycles (Figure 5 I–J).

The genetic ablation of the PDF expressing LN_vs results in a profound reduction in the amplitude of the activity rhythm under gradual temperature cycles, even more severe than those displayed by flies lacking dorsal termini (Figure 5K–L). Flies lacking PDF peptide displayed normal activity rhythms under such temperature cycles (Figs. 5M–N). Consistent with previous studies [42], ablation of PDF-expressing LN_vs did not prevent flies from entraining to step function temperature cycles (Figure S7 A–F). The more severe effects of LN_v ablation under ramping temperature cycles highlights the challenging nature of this constantly and slowly changing time-cue. We conclude that the normal entrainment of activity rhythms to constantly changing temperature cycles requires LN_v neurons but not the peptide transmitter PDF, providing further evidence that the functions of the terminal arborization and the neuropeptide are distinct.

If the dorsal termini are important for the integration of temperature inputs, previous manipulations that abrogated the dorsal termini of the s-LN_vs yet failed to produce circadian output phenotypes should produce clear entrainment phenotypes under gradual temperature cycles. We chose to examine flies over-expressing Fas2 in the LN_vs. As previously described [10], *Pdf-Gal4/UAS-Fas2* flies display a profound and specific loss of the s-LN_v dorsal termini yet display completely normal activity rhythms (Figure S5 and S6A). Under gradually ramping temperature cycles these flies display activity patterns highly reminiscent of those displayed by *Pdf-Gal4/UAS-Unc5 flies* (S6B-D). *Pdf-Gal4/UAS-Fas2* flies also appeared to have weaker rhythms during the free-run following ramping temperature cycles (Figure S6E–F). These results support the hypothesis that the dorsal termini of the s-LN_vs are critical for the integration of temperature inputs for the entrainment of daily activity rhythms.

The s-LN_v dorsal termini puncta are directly inhibited by glutamate.

Previous work has shown that excitation of the glutamatergic $DN1_p$s produces inhibitory responses in the cell bodies and dorsal projections of the s-LN_vs and bath applied glutamate causes hyperpolarization and Ca^{2+} decreases in s-LN_v cell bodies [36]. SEM reconstruction of the s-LN_v dorsal projection revealed that their termini are sparsely dendritic [16]. If the dorsal termini of the s-LN_vs mediate glutamate reception, we would therefore expect them to be directly inhibited by bath-applied glutamate. Direct inhibition is difficult to detect with currently available fluorescent sensors, as changes in fluorescence caused by movement artifacts often rival the small calcium or voltage changes caused by inhibitory responses. This issue is a particularly difficult challenge when attempting to live-image the fine termini of the s-LN_vs, because slight movements in the Z-plane can dramatically alter the intensity of small areas of interest. To address this challenge, we used a resonant scanner to rapidly scan the entire volume of the dorsal termini while co-expressing GFP-based sensors with td-Tomato [43] so that we could objectively define volumes of interest corresponding to the dorsal termini in a manner independent of the fluorescence of our sensors (Figure 6A–C and S8A–B).

We applied glutamate in the presence of 2μM tetrodotoxin (TTX) to inhibit axonal firing and focus on the direct effects of transmitters. Under these conditions, we detected no direct effects of bath-applied glutamate on the fluorescence of GCAMP6f, a Ca^{2+} sensor [44], or

ASAP2f, a voltage sensor that displays fluorescent increases upon hyperpolarization of the membrane [45], even with doses as high as 10mM (Figure S7 J–M). 1mM GABA, which has been previously shown to inhibit the s-LN_vs, also failed to produce measurable fluorescence changes in either of these sensors (Figure S7 J and M), suggesting that, under these conditions, ASAP2f and GCaMP6f are not sufficiently sensitive to detect the direct effects of bath-applied inhibitory neurotransmitters on the dorsal termini. We therefore addressed glutamate receptivity in the s-LN_v dorsal termini by asking if bath-applied glutamate could reduce or abrogate the direct response to cholinergic excitation, an approach that we used previously to address GABAergic inhibition in s-LN_v cell bodies [46].

The dorsal termini are directly responsive to the general cholinergic agonist carbachol (CCh), displaying consistent excitatory increases in Ca^{2+} in response to 30-second bath applications of 0.025mM CCh in the presence of TTX (Figure S7 O and Q). We co-applied 0.025mM CCh with 1mM glutamate for each brain we observed and compared the magnitude of the GCaMP6f response to an immediate 30-second bath application of 0.025 CCh alone (Figure 6D–F and S7 N–Q). All experiments were performed in the presence of TTX. For every brain tested (n = 8), the presence of 1mM glutamate reduced or completely abrogated the direct excitatory response to CCh in the dorsal termini (Figure 6D–F and S N–Q). The same effect of 1mM glutamate was observed in a second series of brains for which 0.01mM CCh stimulation was used (data not shown).

The knockdown of glutamate gated chloride channels in the s-LN_vs results in temperature entrainment deficits.

We hypothesize that sites of daily remodeling in the s-LN_v dorsal termini are required for glutamatergic input from the $DN1_p$ to the s-LN_v and that this input mediates the integration of temperature cycles into the circadian clock neuron network. We therefore predicted that the manipulation of glutamate receptors in the s-LN_vs would result in significant changes in the organization of activity cycles under constantly changing temperature cycles that would be reminiscent of those associated with the absence of s-LN_v dorsal termini. The expression of two independent RNAi constructs targeting distinct sequences of the glutamate gated chloride channel GluClα in the LN_vs resulted in phenotypes that were remarkably similar to those caused by the prevention of s-LN_v dorsal termini development (compare Figure 7A–D to Figs. 5A–C). The expression of GluClα-RNAi in LN_vs resulted in lower amplitude activity rhythms and activity increases that failed to coincide with the daily rise in temperature (Figs. 7A–D), further supporting the notion that the s-LN_vs are critical for the reception of glutamate-mediated temperature inputs. Thus, reducing the expression of GluClα in the s-LN_vs phenocopied the loss of their dorsal terminal arbors, implicating these sites of structural plasticity in the reception of glutamatergic inputs relevant for the integration of temperature into the clock neuron network. The s-LN_vs have previously been shown to express the metabotropic inhibitory glutamate receptor mGluR [47]. RNAi constructs targeting the inhibitory metabotropic glutamate receptor mGluR produced similar deficits in the entrainment to temperature ramps (Figure 7E–H), suggesting that ionotropic and metabotropic glutamate may both mediate glutamatergic temperature inputs to the s-LN_vs.

Discussion

The sites of daily remodeling in the s-LN$_v$s are not required for circadian timekeeping or clock output function.

A significant body of anatomical and genetic evidence supports the longstanding and widely accepted conclusion that the ramified dorsal terminal arbors of these cells are critical sites of circadian output within the fly's timekeeping network (e.g., [14, 16]). We find that flies in which the development of these terminal ramifications has been failed to display changes in PDF-mediated timekeeping or output functions. These unexpected results lead us to conclude that the daily remodeling observed for these neurons is unlikely to mediate circadian output functions. Rather, they suggest that PDF mediated circadian output from the s-LN$_v$s either acts over relatively long distances within the dorsal protocerebrum or that the major sites of circadian output take place in another region of the brain. Indeed, SEM reconstructions of the s-LN$_v$ dorsal projections reveal that PDF is released extrasynaptically in regions unopposed by post-synaptic regions of neighboring neurons [16] and recent work suggests that the accessory medulla may be the critical site of PDF output [48].

There is precedent for the timekeeping and output functions of the circadian system operating in the absence of synaptic connections with the nervous system. In moths, the circadian gating of adult emergence is abolished through the removal of the pupal brain, a deficit that can be rescued by the implantation of a donor brain in the abdomen of brainectomized pupae with the timing of emergence matching that of the species from which the donor brains were taken [49]. The loss of wheel running rhythms in nocturnal rodents caused by the bilateral ablation of the SCN is rescued by the implantation of fetal SCN in the third ventricle of the brain [50], even when the implant is encased in a semi-permeable capsule that prevents the outgrowth of neurons from the implant [51]. In the context of these striking findings it is perhaps not surprising that the proper location of the fine ramifications of the s-LN$_v$s is not required for robust and properly timed circadian rhythms.

The loss of the sites of daily remodeling in the s-LN$_v$s prevents the integration of glutamate mediated time-cues.

Our results indicate the plastic dorsal termini of the s-LN$_v$s are necessary for the normal entrainment of the circadian clock to such temperature cycles and suggest that the puncta of these termini are directly receptive to glutamate. We suggest that preventing the development of dorsal termini prevented the normal pattern and extent of DN1$_p$ glutamatergic synapses onto the medial and lateral extensions of s-LN$_v$ dorsal termini, leading to deficits in the integration of temperature inputs into the circadian clock neuron network. Thus, the sites of structural plasticity in the s-LN$_v$s mediate sensory input and integration in the key set of clock neurons and daily structural changes in these termini likely result in changes in the number and/or strength of inhibitory synapses between the DN1$_p$s and the dorsal termini of the s-LN$_v$s. Though the *Drosophila* clock is robustly reset by pulses of light, only extremely hot or very long pulses of heat reset the phase of the free-running locomotor rhythm [42, 52]. [53]We wonder if the sensitivity of temperature input pathways to s-LN$_v$ dorsal projection structure and the fact that these projections are downscaled over a

significant portion of the circadian cycle [8] might at least partially explain the relative insensitivity of the free-running rhythm to temperature pulses.

Neuronal plasticity likely characterizes sensory input pathways in both insects and mammals.

Neurons within the SCN of the hypothalamus also display marked daily structural changes [23, 24]. Remarkably, the density of glutamatergic synapses onto VIP expressing neurons, cells that mediate functions strikingly similar to those of PDF-expressing LN_vs in the fly, were found to vary across the diurnal cycle [23]. Though the circadian functions of such remodeling have not been determined experimentally for mammals, they are hypothesized to underlie the entrainment of the clock to light/dark cycles [23]. Our work strongly links the sites of daily remodeling in a critical set of clock neurons in the fly with glutamate-mediated input and the integration of environmental time-cues. A canonical property of circadian rhythms is that the effect of environmental perturbation on the free-running system depends on the time at which it is delivered. The same perturbation delivered at various times in the circadian cycle can produce advances, delays, or have no effect on the subsequent phase of the rhythm (e.g., [54]). Given our findings that sites of structural plasticity mediate sensory input into the *Drosophila* clock neurons network, we hypothesize that daily changes in micro-anatomical features of clock containing neurons underlie the gating of such input into the clock neuron networks of both mammals and insects.

STAR METHODS

RESOURCE AVAILABILITY

Lead Contact—Further information and requests for resources and reagents should be directed to and will be fulfilled by the Lead Contact, Orie Shafer (oshafer@gc.cuny.edu).

Materials Availability—All unique/stable reagents generated in this study are available from the Lead Contact without restriction. Further information and requests for resources and reagents should be directed to and will be fulfilled by the Lead Contact, Orie Shafer (oshafer@gc.cuny.edu).

Code Availability Statement—Circular Data Analysis and Visualizations: The GitHub repository contains the R code used to perform the circular data analysis and related visualizations. The source document is the RMarkdown file with Rmd extension, which contains all R code used to generate the rose plots and circular histograms using phase data. We use the R programming environment, and the RStudio IDE for all data analysis and visualizations. The key R library that we used for all circular data analysis and visualizations is circular. The R code used to segment and quantify sensor fluorescence based on tdTomato-defined regions of interest is currently being organized into a user-friendly interface and will be made available on GitHub as soon as possible. The current version is available on request.

EXPERIMENTAL MODEL AND SUBJECT DETAILS

Fly Stocks and husbandry: Flies were reared on cornmeal-sucrose-yeast media under a 12hr:12hr light:dark (LD) cycle at 25 °C for standard LD-DD experiments or under constant darkness at 25 °C for temperature ramp experiments. The following fly lines were used in this study: *;Pdf(BMRJ)-Gal4; ;;Pdf01* and *;UAS-hid/CyO* [15, 55], (provided by P. Taghert, Wash U Med. School), *yw*;*Pdf-LexA*; [56] (provided by M. Rosbash, Brandeis), ;;*Clk4.1M-LexA* [35] (provided by A. Seghal, UPENN); *w;UAS-CD8:GFP*; [57]; *w;;UAS-Dicer-2* (Bloomington Stock Center #24651), w;*UAS-Fas2; (Dr. V. Budnik, UMSS Med. School), w;;UAS-Unc5-HA (Barry Dickson, Janelia Farm)* [28], *UAS-Dscam-TM1-GFP; Pin/CyO*; [58], *;;UAS-Dbt*^{LONG} *myc(27MIC)/(TM3)* (Jeffrey Price, University of Missouri at Kansas City) [59], *w;;20xUAS-GCamp6f* (Bloomington Stock Number 52869, [44]), *w;20xUAS-ASAP2f*; (Bloomington Stock Number 65415, [45]), *w;UAS-tdTomato* (Bloomington Stock Number 35841), *w;LexAop-mCD8GFP;TM2/TM6B,Tb* (Bloomington Stock Number 66545), *;UAS-mGluR-RNAi*; (Vienna Drosophila Resource Center ID 103736), *w;;UAS-mGluR-RNAi* (Vienna Drosophila Resource Center ID 1793), ;*UAS-GluCl*$^{\alpha RNAi}$; (Vienna Drosophila Resource Center ID 107971), ;*UAS-GluCl*$^{\alpha RNAi}$; (Vienna *Drosophila* Resource Center ID 105754).

METHOD DETAILS

Immunocytochemistry: Immunostaining of whole-mount *Drosophila* adult brains was done as previously described (Fernández et al., 2008). Flies were entrained to 12:12 LD cycles at 25°C and dissected brains were fixed in 4% paraformaldehyde for 1 hour at room temperature, blocked with 3% normal goat serum for 1 hour at room temperature, incubated with primary antibodies at 4° C overnight, and rinsed in PBS + 0.3% Triton (PBS-TX). The following antibodies were used: mouse anti-PDF (1:500, Developmental Hybridoma Bank), guinea pig anti-PAP (1:500, provided by Paul Taghert, Wash. U. Med School), rabbit anti-GFP (1:1000, Invitrogen A-6455), and rat anti-PER (1:500). Brains were rinsed of primary five times for 15 minutes or more with high agitation tumbling in PBS-TX and then kept in secondary antibody cocktail at 4° C overnight or for 2 h at room temperature and then rinsed in PBS-TX again as for primary. Alexa Fluor conjugated secondary antibodies (Alexa Fluor 488 and 568 conjugated goat anti-mouse, anti-guinea pig, anti-rabbit, and anti-rat) were diluted 1:1000 (Jackson Immuno Research Labs, West Grove, PA). Brains were rinsed three times in PBS, mounted on a poly-L-lysine coated cover slip, dehydrated/cleared in a graded glycerol series (30%, 50% and 70% glycerol in PBS, 5-min each), and then mounted between coverslip bridges in HardSet Vectashield Mounting Medium (Vector Laboratories, Burlingame, CA). All samples were imaged on an Olympus Fluoview 3000 laser-scanning confocal microscope using either a UplanSApo 20x/0.75 NA or a 60x/1.10 NA W, FUMFL N objective (Olympus, Center Valley, PA). The arbor area and projection length of the s-LN_vs were quantified using the Fiji platform [60] in ImageJ [61]. The length of the dorsal projection was determined by a line drawn from the point at which the s-LN_vs dorsal projection and the posterior optic tract of the l-LN_Vs bifurcate near the accessory medulla to the end of the shortest neurite in control flies or at the distal end of the ‘bundle’ at the dorsal termini of Unc5 or Fas2 expressing s-LN_vs. Area was determined by tracing the perimeter of the entire arbor in a projected Z-series. Imaris (Oxford Instruments, Abingdon, UK) was

used for three dimensional reconstructions of the dorsal termini that were the basis of the quantification of total 3-D arbor spread. PER immunosignals were quantified using Image J as previously described using anti-PAP immunosignal to differentiate between cytoplasmic and nuclear pixels [53].

Live Imaging: *Pdf(M)-Gal4;UAS-tdTomato;UAS-GCaMP6f* or *Pdf(M)-Gal4;UAS-tdTomato;UAS-ASAP2f* flies were anesthetized on ice, immobilized with a minuten pin through the thorax onto a 35mM Sylgard dish, and dissected under ice cold hemolymph-like saline (HL3) consisting of (in mM): 70 NaCl, 5 KCl, 1.5 $CaCl_2$, 20 $MgCl_2$, 10 $NaHCO_3$, 5 trehalose, 115 sucrose, 5 HEPES; pH 7.1 [62]. After dissection of all cuticle and pigmented eye tissue, brains were allowed to adhere to the bottom of poly-lysine coated 35 mm cellular culture dish (Becton Dickenson Labware, Franklin Lakes, NJ) under a drop of HL3 contained within a petri dish perfusion insert placed on the bottom of the dish with double sided adhesive (Bioscience Tools, San Diego, CA). Perfusion flow was established over the brain with a gravity-fed PS-8H perfusion system (Bioscience Tools, San Diego, CA). Test compounds were delivered to mounted brains by switching perfusion flow from the main line of HL3 saline containing 2μM tetrodotoxin citrate (TTX) (Tocris, Bristol, U.K.) to other channels containing agonists diluted in HL3 containing TTX, these included carbachol chloride (Tocris, Bristol, U.K.), L-glutamic acid (Sigma Aldrich, St. Louis) and GABA. All working solutions were pHed to 7.1. For vehicle controls, we perfused HL3 + TTX from a second line.

Live imaging was performed on an Olympus FV3000 laser-scanning microscope with a resonant scanner (Olympus, Center Valley, PA) under a 60x/1.10 NA W, FUMFL N objective (Olympus, Center Valley, PA). Brains were imaged simultaneously for GFP and tdTomato using 488nm and 561nm lasers. The confocal aperture was opened until the optical section was 3 microns. Rapid Z-series were taken through the entire volume of the terminal arbors of the s-LN_vs once every two seconds using three-micron steps. All time-series experiments lasted three minutes. Agonists were applied for 30-seconds starting 15-seconds after the start of each time-series. For transmitter co-application experiments, brains were first exposed to CCh with glutamate and then re-imaged immediately with a second three-minute time-course in which CCh was added by itself. GCaMP6f and ASAP2f fluorescence intensities were monitored for each timepoint on maximum projections of the Z-series within a region of interest outlining the dorsal termini as determined by a segmentation of tdTomato fluorescence using software written in R (available upon request). For each time-course the mean pixel intensities were determined for the region of interest for every time-point and expressed as a proportional change in fluorescence: $\Delta F/F_0$ in which ΔF is the fluorescence intensity value at a given timepoint minus F_0. An average of the intensity values for the first seven timepoints was used for F_0. These values were multiplied by 100 to express values as percent change.

Image Processing: We used imager as the key R library. For the data visualizations, we used ggplot2 and Prism8. The time window for all experiments was 90 time points covering 180 sec.

Max-Intensity Projections: We projected all z-slices from a given z-stack onto a maximum-intensity projection by computing an output image each of whose pixels contained the maximum value over all images in the z-stack at the particular pixel location. The confocal microscope software generated two folders of images for each brain in the experiment. The first folder consisted of images showing the fluorescence response to 0.025mM Carbachol + 1mM Glutamate, and the images are captured in green (GCaMP6f) and red (td-Tomato) channels. The second folder consisted of images showing the fluorescence response to 0.025mM Carbachol alone, and the images were captured again in green (GCaMP6f) and red (td-Tomato) channels. Therefore, each folder had two channels, and each channel has 90 time points and h z-slices for each time point. Thus, the total number of images in the folder is $2 \times 90 \times h$. In particular, if $h = 14$, then we have 2520 images in each folder. We computed the max-intensity projections at each time point for each channel. Thus, we obtained two image lists of 90 projections in the green and red channels for each one of the two folders, corresponding to a particular brain.

Image Segmentation: Next, we computed dynamically (for each time point) an image segmentation of the green channel projections using the red channel projections as a basis for computing the binary pixel set that defines the boundaries of the spatial structure of interest common to both channels. The pixel set computed from the red channel was then superimposed on the green channel for each time point. Once the segmentation of the green channel projection was computed dynamically for each time point, we extracted the pixel values inside the segmented region of the green channel and computed the mean pixel intensity for that time point to obtain the time series of mean pixel intensities for the green channel projections. We repeated the above steps for the green channels in each folder using the corresponding red channels to compute dynamically the pixel sets and superimposed them on the green channels in order to compute the mean pixel intensities of the green channels.

We computed the binary pixel set from the grayscale image of the red channel by first applying isotropic blurring, which creates a region with better defined boundaries, and this process was controlled by one parameter (the standard deviation of the blur as a number of pixels). We then set a threshold, which was also controlled by one parameter. These were the two key parameters that controlled the segmentation. For finer control of the segmentation, we also added a process of growing a pixel set through morphological dilation, controlled by one parameter. In addition, we used the built-in functionality in the imager library to split pixel sets into connected components. The benefit of this splitting comes from the ability to keep only relevant blobs based on the total luminosity of the components (being the free parameter here), thus ignoring small, irrelevant islands that may be captured by the main segmentation processes. We calibrated all four segmentation parameters using the red channels.

Curve Normalizations: We used the time series $(F_t)_{t=1}^{90}$ of mean pixel intensities, computed for the green channel of each image folder using binary pixel sets calibrated by the red channel, to get the change in the mean pixel intensities relative to a base level F_0,

computed as the average of the first 7 mean pixel intensities from the original time series, i.e. $F_0 = \frac{1}{7}\sum_{t=1}^{7} F_t$. Thus, the dimensionless relative change at time point is given by:

$$R_t = \frac{\Delta F_t}{F_0} = \frac{F_t - F_0}{F_0}$$

4-point Running Average: We smoothed out the time series of the relative change $(R_t)_{t=1}^{90}$ by applying a 4-point running average in order to filter the short-term fluctuations and emphasize long-term trends. The first element of the running average was obtained by taking the average of the first 4 elements from the relative change series. Then the 4-point window was shifted forward by one time point and the local average was computed again, and so on. However, the smoothed series thus obtained had a length of 87, three less than the original series, which presented difficulties when it came to visualizations. There are a number of running average algorithms that correct this issue and return a vector of the same size as the original one by providing a rule for filling the missing numbers. The rule that we used was to fill both ends of the smoothed series by using the corresponding ends of the original series.

The Area Under the Curve (AUC): We computed the positive area over the time interval [16,76] [sec] (to capture the 60 sec course of treatment), under the smoothed relative change curve $y(t)$, by approximating the area using trapezoids. To ensure that we computed only the positive area under the curve $y(t)$, we considered only the positive part of the curve $y(t)^+ = \max(y(t),0)$, when we sum the areas of the trapezoids under the curve over the given interval.

Locomotor activity rhythm recording and analysis: Locomotor activity rhythms of adult male flies were recorded using DAM2 *Drosophila* Activity Monitors (TriKinetics, Waltham, MA). Three- to five-day old flies were placed individually in Trikinetics capillary tubes containing 2% agar- 4% sucrose food at one end sealed with paraffin wax, plugged with a small length of yarn, and loaded onto the DAM2 monitors for locomotor activity recording. For standard LD entrainment and transfer to constant darkness (DD) free-run experiments, flies were entrained to 12:12 LD cycles for at least five days, and then released into constant darkness (DD) for at least eight days, at a constant temperature of 25°C. Activity counts were collected in 1-minute bins that were subsequently summed into 30-minute bins for the time-series analysis of locomotor activity.

Averaged population activity profiles of specific genotypes in LD were generated in Matlab (MathWorks, Natick). First, activity levels were normalized for individual flies, by setting the average activity level for all 30-min bins across the last four days in LD equal to 1.0. Population averages of this normalized activity were then determined for each 30-min bin over the number of LD cycles indicated in the results and Figure legends. Finally, the population averages for the LD cycles were averaged into a single representative 24-hour day, which are displayed as either histograms or line plots.

Morning anticipation of light transitions under 12:12 LD was quantified by fitting 30-min binned beam crossing data over the last six hours of the night, with a least-squares linear

regression. The beam crossing data for this six-hour window was averaged for the last 3 days of LD for individual flies and then normalized relative total activity for each fly within this window. These data were plotted for single flies in Matlab using the 'scatter' plotting function along with the least-squares regression lines fit to the average six-hour activity time-courses (Supplemental Figs. S2 and S3). These scatter plots and regressions were overlaid with a line representing the average of the all individual fly regression lines. The slopes of individual regression lines were used as a metric of morning anticipation for single flies. The same approach was applied to the six hours preceding lights-on for the quantification of evening anticipation.

The phases of morning and evening peaks of individual flies on day one of DD were determined as previously described [30]. Briefly, individual time-courses of beam crossings/30min through the first day under DD were subjected to a zero-phase Butterworth filter to diminish oscillations with periods of less than 20 hours [63]. The 'Findpeaks' function in the Signal Processing Toolbox of Matlab was used for each fly's filtered activity plot to identify the morning and evening peaks of activity, and their corresponding phases expressed as Circadian Time (CT). The morning and evening peak phases of experimental genotypes were compared to those of their parental controls using a Kruskal-Wallis one-way ANOVA and Dunn's multiple comparison test. A summary of all pairwise comparisons is listed in Supplementary Table S1. In the case of the *w;Pdf(BMRJ)-Gal4/+;UAS-Dbt^{LONG}/UAS-Unc5 flies*, we compared the behavior of these flies to all of the relevant single P-element heterozygotes and all double heterozygote combinations.

To examine entrainment to naturalistic, gradually ramping temperature cycles, flies were reared under constant darkness (DD) at 25°C and then entrained to temperature cycles that gradually and constantly increased from 20 °C to 28 °C from ZT 00 to ZT 12 and gradually and constantly decreased from 28 °C to 20 °C from ZT 12–00 under DD. Flies were entrained under such temperature cycles for eight days. Averaged individual population activity plots were constructed for the last three days of temperature entrainment. The tracking of daily activity with rising environmental temperature was quantified as a "Heating Index" as described previously [37]. Briefly, the heating index is the Pearson product-moment correlation coefficient between the mid-day rise in temperature and locomotor activity and was calculated for activity/temperature between ZT05 and ZT11. Under the temperature conditions used here, flies displayed a startle response at the onset of heating that was dwarfed by the daily peak of activity that coincided with the warmest daily temperatures.

QUANTIFICATION AND STATISTICAL ANALYSIS

The n, mean, standard deviation, and standard errors for all datasets are described in Table S1. The error bars displayed in all figures represent standard error of the mean (SEM). We tested each dataset for normality using a D'Agostino- Pearson normality test in GraphPad Prism 8.0. For parametric datasets, we used unpaired Student's t tests and one-way ANOVA with Tukey's multiple comparisons test. For non-parametric datasets, we used Mann-Whitney tests and the Kruskal-Wallis tests with Dunn's multiple comparisons tests. The results of the normality tests and the statistical tests employed for all data sets are described

in Table S1. Statistical tests were performed using GraphPad Prism 8.0, except for the circular statistics tests that are described in this section below. Asterisks indicate statistical significance, where *p < 0.05, **p < 0.01, and ***p < 0.001.

We analyzed free-running activity rhythms using ClockLab software from Actimetrics (Wilmette, IL) as previously described [31]. In brief, rhythmicity, rhythmic power, and free-running period of individual flies were analyzed using Clocklab's χ-square periodogram function implemented in ClockLab, based on a confidence level of 0.01 [64]. For all genotypes tested, significant periodicities between 14 and 34 hours were considered. For individuals that displayed more than one periodicity with a peak over significance, only the highest amplitude period was used for the determination of average periods displayed in Figure 3 and Table S1. For each peak in the χ-square periodogram, Clock Lab returns a "Power" value and a "Significance" value. As previously described [31, 65], "Rhythmic Power" was calculated by subtracting the Significance value from the Power value of the predominant peak for every fly designated as rhythmic, and was considered "0" for flies that failed to display a peak periodicity above significance.

For circular statistics and rose plots, we transformed the negative and positive phases into proper hours on the 00–24h time scale by taking all phases modulo 24, and then converting the proper hours into radians. The zero-hour ZT00 is set at 24h, or 2π radians. We then applied the Watson two-sample test to determine whether the phases for control and experimental lines are significantly different. Watson's non-parametric two sample U 2 statistics provides a criterion to test whether two samples differ significantly from each other. We performed nine tests using both the *Watson-Wheeler Test for Homogeneity of Angles* and the *Watson's Two- Sample Test of Homogeneity* from the circular R library, designed and implemented for analyzing circular data. For both tests, the null hypothesis is that the two samples of angles come from the same underlying population.

Highlights

- Loss of the presumed major sites of circadian output do not affect circadian rhythms.
- Loss of these sites prevents the normal entrainment of rhythms to temperature cycles.
- Plastic neural structures mediate glutamatergic clock inputs in mammals and insects.
- Structural changes likely alter the strength of sensory inputs to clock neurons.

Supplementary Material

Refer to Web version on PubMed Central for supplementary material.

Acknowledgments:

We thank Paul Taghert and Rae Silver for useful comments on this manuscript. We also thank Paul Taghert, Bing Ye and Alex Keene for useful discussions about the work and Barry Dickson, Greg Bashaw, Paul Taghert, Michel Rosbash, Vivian Budnick, Tom Clandinin, Bing Ye, and the Bloomington *Drosophila* Stock Center for sharing fly lines. The authors would like to acknowledge the Live Imaging and Bioenergetics core facility at the CUNY Advanced Science Research Center for instrument use, and scientific and technical assistance and its director Dr. Ye He for sharing her expertise and for her assistance in the use of Imaris software. We also thank the members of the Fernández and Shafer labs for comments on the text. The work was supported by a National Institutes of Health

NINDS grant (R01NS077933) and an NSF IOS grant (1354046) to O.T.S, start-up funds from the Graduate Center at City University of New York to O.T.S., and start-up funds from Barnard College to M.P.F.

References:

1. Roenneberg T, Daan S, and Merrow M (2003). The Art of Entrainment. Journal of Biological Rhythms 18, 183–194. [PubMed: 12828276]
2. Roenneberg T, and Merrow M (2016). The Circadian Clock and Human Health. Current Biology 26, R432–R443. [PubMed: 27218855]
3. Herzog ED (2007). Neurons and networks in daily rhythms. Nature Reviews Neuroscience 8, 790. [PubMed: 17882255]
4. Hastings MH, Maywood ES, and Brancaccio M (2018). Generation of circadian rhythms in the suprachiasmatic nucleus. Nature Reviews Neuroscience 19, 453–469. [PubMed: 29934559]
5. Golombek DA, and Rosenstein RE (2010). Physiology of Circadian Entrainment. Physiological Reviews 90, 1063–1102. [PubMed: 20664079]
6. Bosler O, Girardet C, Franc J-L, Becquet D, and François-Bellan A-M (2015). Structural plasticity of the circadian timing system. An overview from flies to mammals. Frontiers in Neuroendocrinology 38, 50–64. [PubMed: 25703789]
7. Krzeptowski W, Hess G, and Pyza E (2018). Circadian Plasticity in the Brain of Insects and Rodents. Frontiers in Neural Circuits 12.
8. Fernández MP, Berni J, and Ceriani MF (2008). Circadian Remodeling of Neuronal Circuits Involved in Rhythmic Behavior. PLOS Biology 6, e69. [PubMed: 18366255]
9. Petsakou A, Sapsis, Themistoklis P, and Blau J (2015). Circadian Rhythms in Rho1 Activity Regulate Neuronal Plasticity and Network Hierarchy. Cell 162, 823–835. [PubMed: 26234154]
10. Sivachenko A, Li Y, Abruzzi, Katharine C, and Rosbash M (2013). The Transcription Factor Mef2 Links the Drosophila Core Clock to Fas2, Neuronal Morphology, and Circadian Behavior. Neuron 79, 281–292. [PubMed: 23889933]
11. Gorostiza EA, Depetris-Chauvin A, Frenkel L, Pírez N, and Ceriani María F. (2014). Circadian Pacemaker Neurons Change Synaptic Contacts across the Day. Current Biology 24, 2161–2167. [PubMed: 25155512]
12. Depetris-Chauvin A, Fernández-Gamba Á, Gorostiza EA, Herrero A, Castaño EM, and Ceriani MF (2014). Mmp1 Processing of the PDF Neuropeptide Regulates Circadian Structural Plasticity of Pacemaker Neurons. PLOS Genetics 10, e1004700. [PubMed: 25356918]
13. Gunawardhana KL, and Hardin PE (2017). VRILLE Controls PDF Neuropeptide Accumulation and Arborization Rhythms in Small Ventrolateral Neurons to Drive Rhythmic Behavior in Drosophila. Current Biology 27, 3442–3453.e3444. [PubMed: 29103936]
14. Helfrich-Förster C (1998). Robust circadian rhythmicity of Drosophila melanogaster requires the presence of lateral neurons: a brain-behavioral study of disconnected mutants. Journal of Comparative Physiology A 182, 435–453.
15. Renn SCP, Park JH, Rosbash M, Hall JC, and Taghert PH (1999). A pdf Neuropeptide Gene Mutation and Ablation of PDF Neurons Each Cause Severe Abnormalities of Behavioral Circadian Rhythms in Drosophila. Cell 99, 791–802. [PubMed: 10619432]
16. Yasuyama K, and Meinertzhagen IA (2010). Synaptic connections of PDF-immunoreactive lateral neurons projecting to the dorsal protocerebrum of Drosophila melanogaster. Journal of Comparative Neurology 518, 292–304. [PubMed: 19941354]
17. Aton SJ, Colwell CS, Harmar AJ, Waschek J, and Herzog ED (2005). Vasoactive intestinal polypeptide mediates circadian rhythmicity and synchrony in mammalian clock neurons. Nature Neuroscience 8, 476. [PubMed: 15750589]
18. Colwell CS, Michel S, Itri J, Rodriguez W, Tam J, Lelievre V, Hu Z, Liu X, and Waschek JA (2003). Disrupted circadian rhythms in VIP- and PHI-deficient mice. American Journal of Physiology-Regulatory, Integrative and Comparative Physiology 285, R939–R949.
19. Hyun S, Lee Y, Hong S-T, Bang S, Paik D, Kang J, Shin J, Lee J, Jeon K, Hwang S, et al. (2005). Drosophila GPCR Han Is a Receptor for the Circadian Clock Neuropeptide PDF. Neuron 48, 267–278. [PubMed: 16242407]

20. Lear BC, Merrill CE, Lin J-M, Schroeder A, Zhang L, and Allada R (2005). A G Protein-Coupled Receptor, groom-of-PDF, Is Required for PDF Neuron Action in Circadian Behavior. Neuron 48, 221–227. [PubMed: 16242403]
21. Mertens I, Vandingenen A, Johnson EC, Shafer OT, Li W, Trigg JS, De Loof A, Schoofs L, and Taghert PH (2005). PDF Receptor Signaling in Drosophila Contributes to Both Circadian and Geotactic Behaviors. Neuron 48, 213–219. [PubMed: 16242402]
22. Becquet D, Girardet C, Guillaumond F, François-Bellan A-M, and Bosler O (2008). Ultrastructural plasticity in the rat suprachiasmatic nucleus. Possible involvement in clock entrainment. Glia 56, 294–305. [PubMed: 18080293]
23. Girardet C, Blanchard M-P, Ferracci G, Lévêque C, Moreno M, François-Bellan A-M, Becquet D, and Bosler O (2010). Daily changes in synaptic innervation of VIP neurons in the rat suprachiasmatic nucleus: contribution of glutamatergic afferents. European Journal of Neuroscience 31, 359–370. [PubMed: 20074215]
24. LeSauter J, Bhuiyan T, Shimazoe T, and Silver R (2009). Circadian Trafficking of Calbindin-ir in Fibers of SCN Neurons. Journal of Biological Rhythms 24, 488–496. [PubMed: 19926808]
25. Cusumano P, Biscontin A, Sandrelli F, Mazzotta GM, Tregnago C, De Pittà C, and Costa R (2018). Modulation of miR-210 alters phasing of circadian locomotor activity and impairs projections of PDF clock neurons in Drosophila melanogaster. PLOS Genetics 14, e1007500. [PubMed: 30011269]
26. Helfrich-Förster C (1997). Development of pigment-dispersing hormoneimmunoreactive neurons in the nervous system of Drosophila melanogaster. Journal of Comparative Neurology 380, 335–354. [PubMed: 9087517]
27. Helfrich-Förster C (1995). The period clock gene is expressed in central nervous system neurons which also produce a neuropeptide that reveals the projections of circadian pacemaker cells within the brain of Drosophila melanogaster. Proceedings of the National Academy of Sciences 92, 612–616.
28. Keleman K, and Dickson BJ (2001). Short- and Long-Range Repulsion by the Drosophila Unc5 Netrin Receptor. Neuron 32, 605–617. [PubMed: 11719202]
29. Stoleru D, Peng Y, Nawathean P, and Rosbash M (2005). A resetting signal between Drosophila pacemakers synchronizes morning and evening activity. Nature 438, 238. [PubMed: 16281038]
30. Yao Z, Bennett AJ, Clem JL, and Shafer OT (2016). The Drosophila Clock Neuron Network Features Diverse Coupling Modes and Requires Network-wide Coherence for Robust Circadian Rhythms. Cell Reports 17, 2873–2881. [PubMed: 27974202]
31. Yao Z, and Shafer OT (2014). The Drosophila Circadian Clock Is a Variably Coupled Network of Multiple Peptidergic Units. Science 343, 1516–1520. [PubMed: 24675961]
32. Chatterjee A, Lamaze A, De J, Mena W, Chélot E, Martin B, Hardin P, Kadener S, Emery P, and Rouyer F (2018). Reconfiguration of a Multi-oscillator Network by Light in the Drosophila Circadian Clock. Current Biology 28, 2007–2017.e2004. [PubMed: 29910074]
33. Shafer OT, and Taghert PH (2009). RNA-Interference Knockdown of Drosophila Pigment Dispersing Factor in Neuronal Subsets: The Anatomical Basis of a Neuropeptide's Circadian Functions. PLOS ONE 4, e8298. [PubMed: 20011537]
34. Zhang L, Chung BY, Lear BC, Kilman VL, Liu Y, Mahesh G, Meissner R-A, Hardin PE, and Allada R (2010). DN1p Circadian Neurons Coordinate Acute Light and PDF Inputs to Produce Robust Daily Behavior in Drosophila. Current Biology 20, 591–599. [PubMed: 20362452]
35. Cavanaugh Daniel J., Geratowski Jill D., Wooltorton Julian R.A., Spaethling Jennifer M., Hector Clare E., Zheng X, Johnson Erik C., Eberwine James H., and Sehgal A (2014). Identification of a Circadian Output Circuit for Rest:Activity Rhythms in Drosophila. Cell 157, 689–701. [PubMed: 24766812]
36. Guo F, Yu J, Jung HJ, Abruzzi KC, Luo W, Griffith LC, and Rosbash M (2016). Circadian neuron feedback controls the Drosophila sleep–activity profile. Nature 536, 292. [PubMed: 27479324]
37. Yadlapalli S, Jiang C, Bahle A, Reddy P, Meyhofer E, and Shafer OT (2018). Circadian clock neurons constantly monitor environmental temperature to set sleep timing. Nature 555, 98. [PubMed: 29466329]

38. Chen C, Buhl E, Xu M, Croset V, Rees JS, Lilley KS, Benton R, Hodge JJL, and Stanewsky R (2015). Drosophila Ionotropic Receptor 25a mediates circadian clock resetting by temperature. Nature 527, 516. [PubMed: 26580016]
39. Chen C, Xu M, Anantaprakorn Y, Rosing M, and Stanewsky R (2018). nocte Is Required for Integrating Light and Temperature Inputs in Circadian Clock Neurons of Drosophila. Curr Biol 28, 1595–1605 e1593. [PubMed: 29754901]
40. Roessingh S, Rosing M, Marunova M, Ogueta M, George R, Lamaze A, and Stanewsky R (2019). Temperature synchronization of the Drosophila circadian clock protein PERIOD is controlled by the TRPA channel PYREXIA. Commun Biol 2, 246. [PubMed: 31286063]
41. Currie J, Goda T, and Wijnen H (2009). Selective entrainment of the Drosophilacircadian clock to daily gradients in environmental temperature. BMC Biology 7, 49. [PubMed: 19671128]
42. Busza A, Murad A, and Emery P (2007). Interactions between circadian neurons control temperature synchronization of Drosophila behavior. J Neurosci 27, 10722–10733. [PubMed: 17913906]
43. Shaner NC, Campbell RE, Steinbach PA, Giepmans BN, Palmer AE, and Tsien RY (2004). Improved monomeric red, orange and yellow fluorescent proteins derived from Discosoma sp. red fluorescent protein. Nat Biotechnol 22, 1567–1572. [PubMed: 15558047]
44. Chen T-W, Wardill TJ, Sun Y, Pulver SR, Renninger SL, Baohan A, Schreiter ER, Kerr RA, Orger MB, Jayaraman V, et al. (2013). Ultrasensitive fluorescent proteins for imaging neuronal activity. Nature 499, 295. [PubMed: 23868258]
45. Chamberland S, Yang HH, Pan MM, Evans SW, Guan S, Chavarha M, Yang Y, Salesse C, Wu H, Wu JC, et al. (2017). Fast two-photon imaging of subcellular voltage dynamics in neuronal tissue with genetically encoded indicators. Elife 6.
46. Lelito KR, and Shafer OT (2012). Reciprocal cholinergic and GABAergic modulation of the small ventrolateral pacemaker neurons of Drosophila's circadian clock neuron network. J Neurophysiol 107, 2096–2108. [PubMed: 22279191]
47. Collins B, Kaplan HS, Cavey M, Lelito KR, Bahle AH, Zhu Z, Macara AM, Roman G, Shafer OT, and Blau J (2014). Differentially Timed Extracellular Signals Synchronize Pacemaker Neuron Clocks. PLOS Biology 12, e1001959. [PubMed: 25268747]
48. Schlichting M, Menegazzi P, Lelito KR, Yao Z, Buhl E, Dalla Benetta E, Bahle A, Denike J, Hodge JJ, Helfrich-Förster C, et al. (2016). A Neural Network Underlying Circadian Entrainment and Photoperiodic Adjustment of Sleep and Activity in Drosophila. The Journal of Neuroscience 36, 9084–9096. [PubMed: 27581451]
49. Truman JW, and Riddiford LM (1970). Neuroendocrine Control of Ecdysis in Silkmoths. Science 167, 1624–1626. [PubMed: 17746371]
50. Lehman M, Silver R, Gladstone W, Kahn R, Gibson M, and Bittman E (1987). Circadian rhythmicity restored by neural transplant. Immunocytochemical characterization of the graft and its integration with the host brain. The Journal of Neuroscience 7, 1626–1638. [PubMed: 3598638]
51. Silver R, LeSauter J, Tresco PA, and Lehman MN (1996). A diffusible coupling signal from the transplanted suprachiasmatic nucleus controlling circadian locomotor rhythms. Nature 382, 810–813. [PubMed: 8752274]
52. Edery I, Rutila J, and Rosbash M (1994). Phase shifting of the circadian clock by induction of the Drosophila period protein. Science 263, 237–240. [PubMed: 8284676]
53. Shafer OT, Rosbash M, and Truman JW (2002). Sequential Nuclear Accumulation of the Clock Proteins Period and Timeless in the Pacemaker Neurons of Drosophila melanogaster. The Journal of Neuroscience 22, 5946–5954. [PubMed: 12122057]
54. De Coursey PJ (1960). Daily Light Sensitivity Rhythm in a Rodent. Science 131, 33–35. [PubMed: 13814727]
55. Park JH, Helfrich-Förster C, Lee G, Liu L, Rosbash M, and Hall JC (2000). Differential regulation of circadian pacemaker output by separate clock genes in Drosophila. Proceedings of the National Academy of Sciences 97, 3608–3613.
56. Shang Y, Griffith LC, and Rosbash M (2008). Light-arousal and circadian photoreception circuits intersect at the large PDF cells of the Drosophila brain. Proceedings of the National Academy of Sciences 105, 19587–19594.

57. Lee T, and Luo L (1999). Mosaic Analysis with a Repressible Cell Marker for Studies of Gene Function in Neuronal Morphogenesis. Neuron 22, 451–461. [PubMed: 10197526]
58. Wang J, Ma X, Yang JS, Zheng X, Zugates CT, Lee C-HJ, and Lee T (2004). Transmembrane/Juxtamembrane Domain-Dependent Dscam Distribution and Function during Mushroom Body Neuronal Morphogenesis. Neuron 43, 663–672. [PubMed: 15339648]
59. Muskus MJ, Preuss F, Fan J-Y, Bjes ES, and Price JL (2007). Drosophila DBT Lacking Protein Kinase Activity Produces Long-Period and Arrhythmic Circadian Behavioral and Molecular Rhythms. Molecular and Cellular Biology 27, 8049–8064. [PubMed: 17893330]
60. Schindelin J, Arganda-Carreras I, Frise E, Kaynig V, Longair M, Pietzsch T, Preibisch S, Rueden C, Saalfeld S, Schmid B, et al. (2012). Fiji: an open-source platform for biological-image analysis. Nature Methods 9, 676. [PubMed: 22743772]
61. Schneider CA, Rasband WS, and Eliceiri KW (2012). NIH Image to ImageJ: 25 years of image analysis. Nature Methods 9, 671. [PubMed: 22930834]
62. Stewart BA, Atwood HL, Renger JJ, Wang J, and Wu C-F (1994). Improved stability of Drosophila larval neuromuscular preparations in haemolymph-like physiological solutions. Journal of Comparative Physiology A 175, 179–191.
63. Levine JD, Funes P, Dowse HB, and Hall JC (2002). Signal analysis of behavioral and molecular cycles. BMC Neuroscience 3, 1. [PubMed: 11825337]
64. Sokolove PG, and Bushell WN (1978). The chi square periodogram: Its utility for analysis of circadian rhythms. Journal of Theoretical Biology 72, 131–160. [PubMed: 566361]
65. Pfeiffenberger C, Lear BC, Keegan KP, and Allada R (2010). Processing Sleep Data Created with the Drosophila Activity Monitoring (DAM) System. Cold Spring Harbor Protocols 2010, pdb.prot5520.

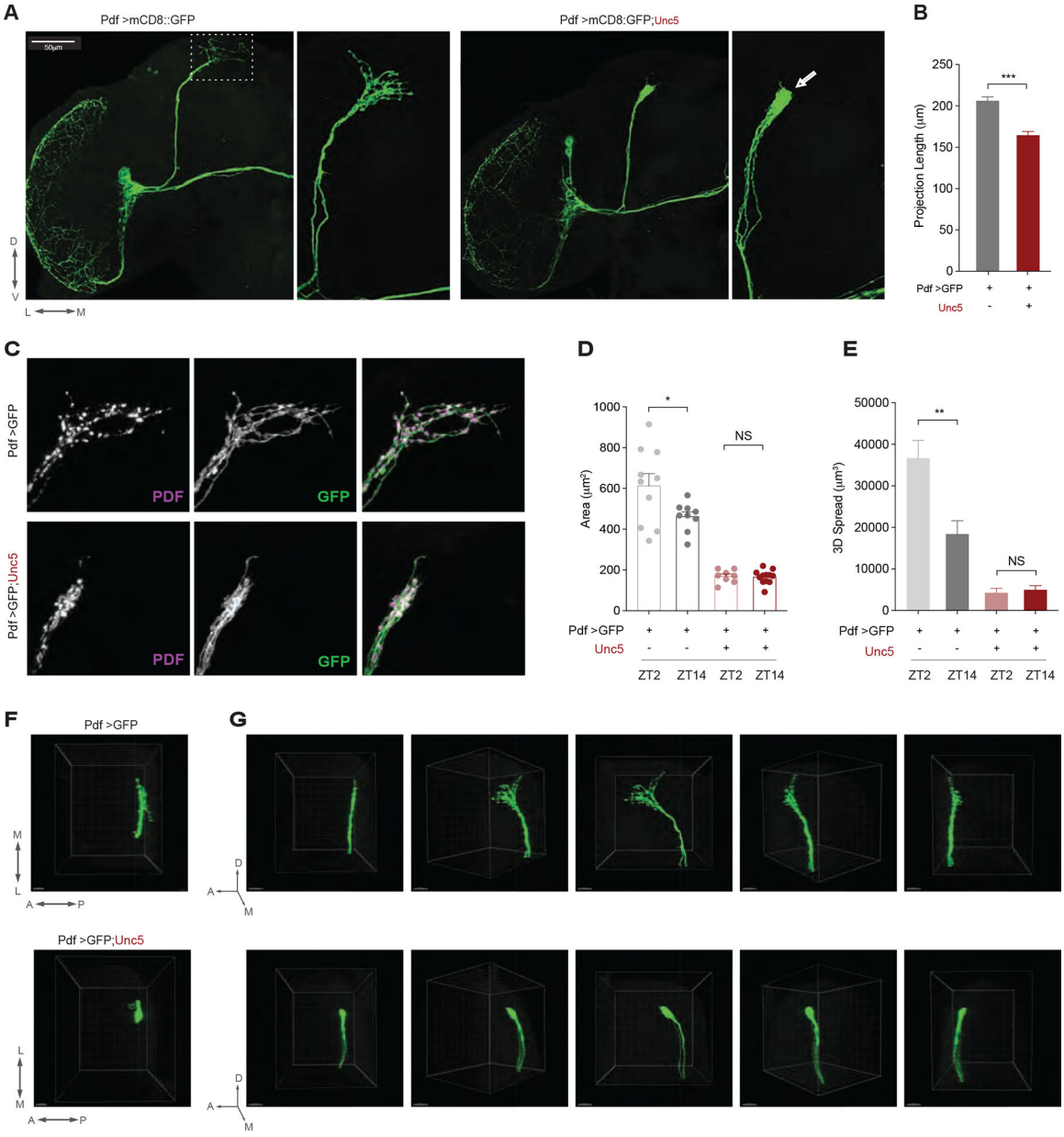

Figure 1. Overexpression of the axon guidance receptor Unc5 eliminates the dorsal arbor from the s-LN$_v$s.

(**A**) Representative confocal images of an anti-GFP immunostaining showing the left hemispheres of a ;*Pdf-Gal4/UAS-mCD8::GFP*; (left panels) and ;*Pdf-Gal4/UAS-mCD8::GFP;UAS-Unc5/+* (right panels) showing a hemisphere of the adult central brain (left sides) and a magnified image of the s-LN$_v$s projections extending into the dorsal protocerebrum (right sides). Scale bar 50µm. Dorsal, ventral, medial, and lateral directions indicated below the left panel. l-LN$_v$s indicate the large ventral lateral neurons, s-LN$_v$s indicate the small ventral lateral neurons, DP indicates the dorsal projection, OL the medulla of the optic lobe, and OT, the posterior optic tract. Arrow in the small right panel indicates loss of termini. The triangle indicates a slight defasciculation of the dorsal projection. (**B**) Quantification of dorsal projection length for the genotypes shown in A. (**C**) Confocal

reconstructions of the dorsal termini of the s-LN_vs in the dorsal protocerebrum of the genotypes shown in A. The left column shows PDF, the middle column anti-GFP, and the right merged micrographs with PDF in magenta and GFP in green. (**D**) Quantification of the effects of Unc5 expression on brain area (i.e., X-Y spread) innervated by the dorsal termini in a collapsed Z-series from a posterior aspect and **(E)** The total three-dimensional spread of the dorsal termini. (**F**) View of the dorsal termini of the genotypes shown in A through the dorsal surface of the brain. Scale bars = 15M. (**G**) Comparison of 180 degree rotations of the dorsal projections of the genotypes shown in A. Panels represent rotations of the projected Z-series starting from a lateral view and ending with a medial view of the projections. Asterisks indicate significant differences. ** $P < 0.01$, *** $P < 0.001$. Error bars represent the standard error of the mean (SEM). See Table S1 for statistical information and sample sizes. See also Figure S1

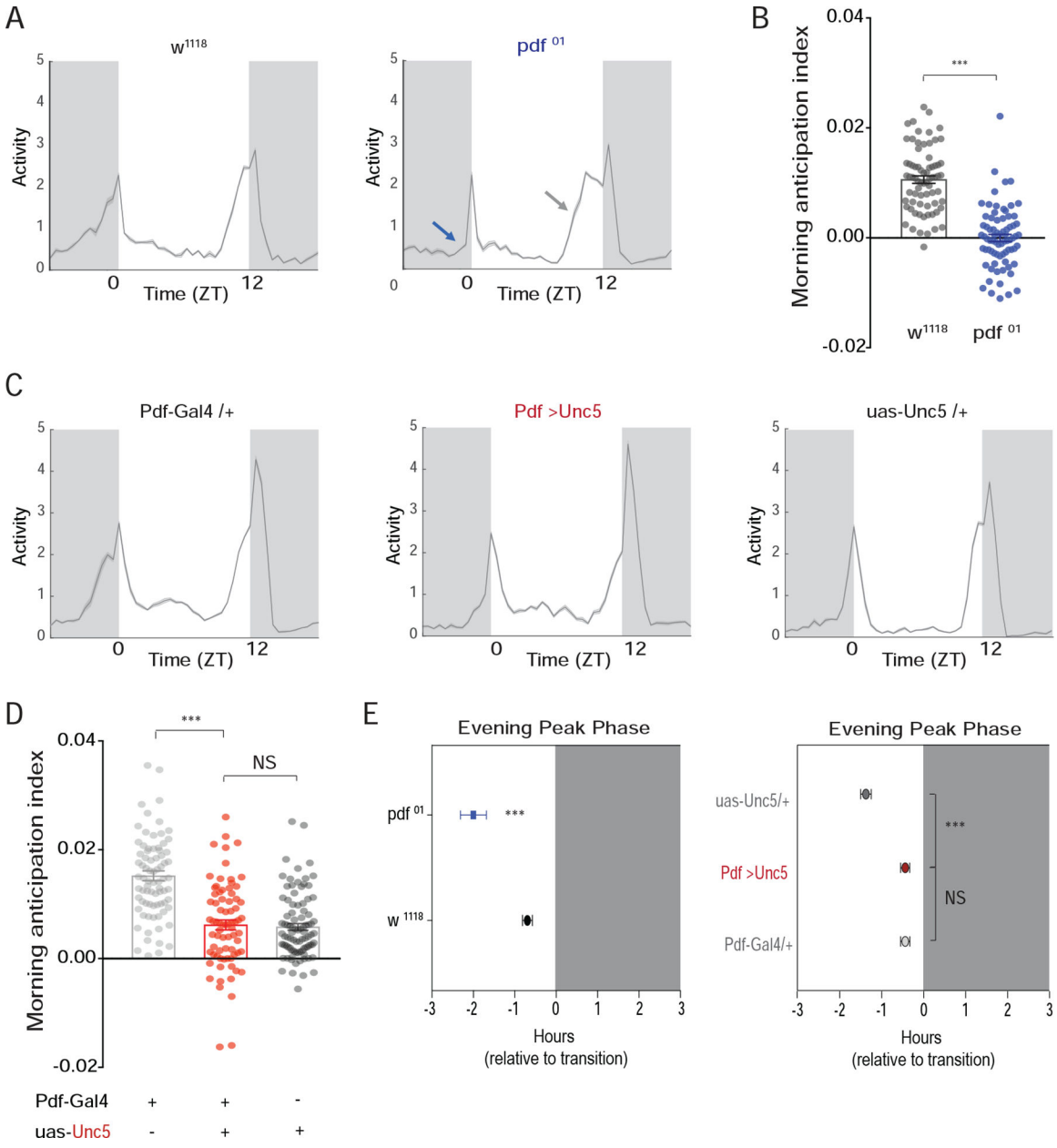

Figure 2. s-LN$_v$ dorsal arbors are not required for PDF dependent behavioral outputs under light/dark conditions.

(**A**) Population averaged activity profiles of wild-type (WT) and *Pdf^{01}* mutant flies under a 12h:12h LD cycle. *Pdf^{01}* mutants lack morning anticipation (blue arrow) and exhibit an advanced evening peak of activity (gray arrow) [15]. (**B**) Morning anticipation differs significantly between WT and *Pdf^{01}* flies. (**C**) Population averaged activity profiles of *;Pdf-Gal4/+;UAS-Unc5/+* flies and their heterozygous parental controls reveal no *Pdf^{01}*-like effects on morning or evening peaks of activity. (**D**) *;Pdf-Gal4/+;UAS-Unc5/+* flies do not differ significantly from their parental controls in morning anticipation. (**E**) *;Pdf-Gal4/+;UAS-Unc5/+* flies also fail to display *Pdf^{01}* like evening peak phenotypes. Average

evening peak phases are displayed +/− SEM. “0” marks the time of lights-off. Dark gray indicates night. See Table S1 for sample sizes and statistics. See also Figures S2 and S3.

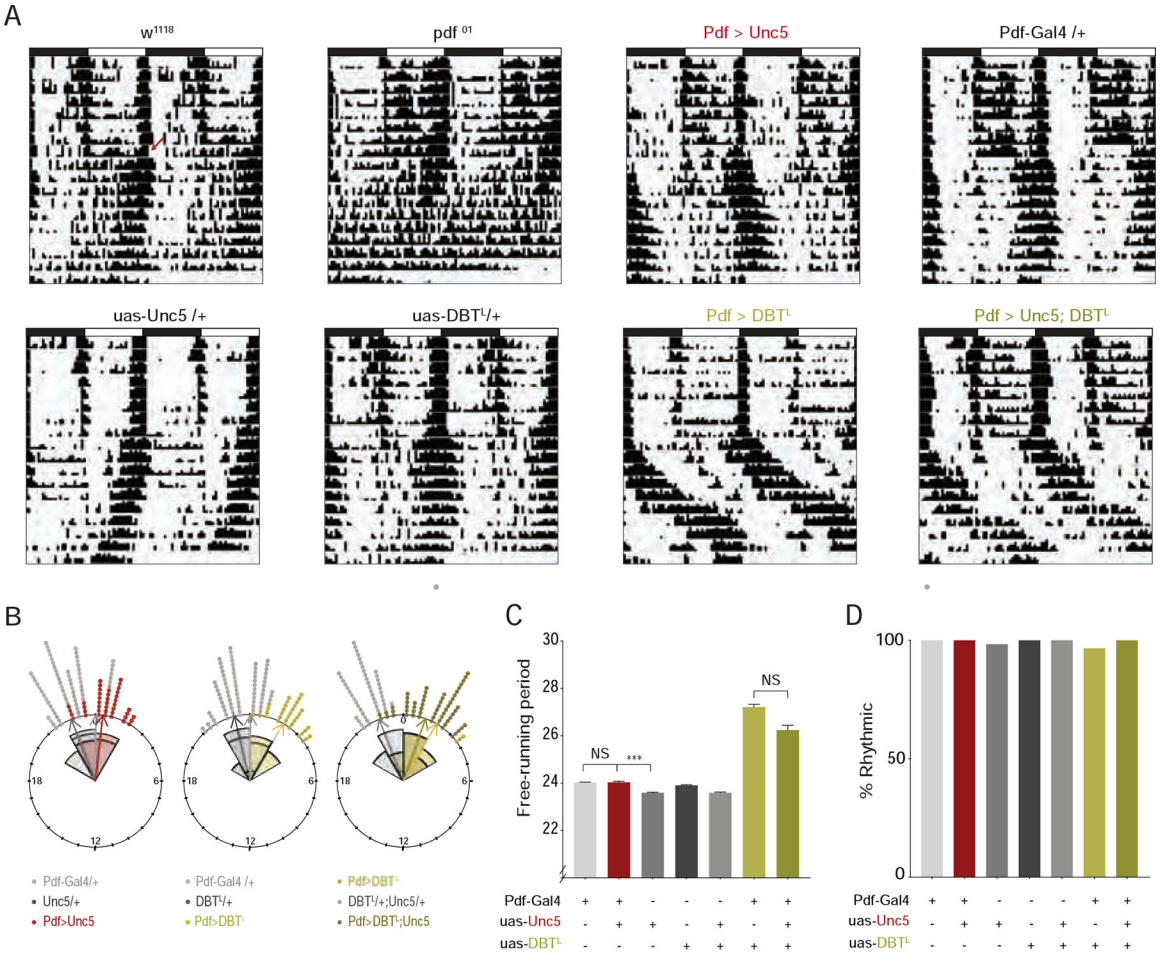

Figure 3. s-LN$_v$s lacking dorsal termini maintain their control of systemic circadian timekeeping.

(**A**) Representative double plotted actograms for flies under 8 days of LD entrainment followed by 10 days of free-running under constant darkness and temperature (DD). Both ;*Pdf-Gal4/+;UAS-Dbt^{LONG}/+* and ;*Pdf-Gal4/+;UAS-Dbt^{LONG}/UAS-Unc5* flies exhibit significantly lengthened free-running periods. Red arrow in top left actogram indicates transition to DD. (**B**) Rose plots of evening activity peaks on the first day of DD for the genotypes indicated. “0” marks the time 24-hours after the final lights-on event. Control *;;uas-Unc5/+* flies displayed relatively early evening peak phases, but experimental *;Pdf-Gal4/+;uas-Unc5/+* flies did not differ from *;Pdf-Gal4/+* controls (left plot). The expression of *Dbt^{LONG}* in the LN$_v$s results in a significantly delayed evening peak (middle plot). The co-expression of *Unc5* with *Dbt^{LONG}* in the Pdf-expressing neurons did not prevent the delay of the evening peak (right plot). (**C**) Mean free-running period for seven days of DD. The endogenous periods of ;*Pdf-Gal4/+;UAS-Dbt^{LONG}/+* and ;*Pdf-Gal4/+;UAS-Dbt^{LONG}/UAS-Unc5/* flies are not significantly different and are significantly longer than all their parental control lines. (**D**) The percentage of flies displaying significant circadian periodicity under DD following entrainment to LD cycles. No significant differences were found among any of the genotypes shown. See also Table S1 for statistical information and sample sizes and Figure S4.

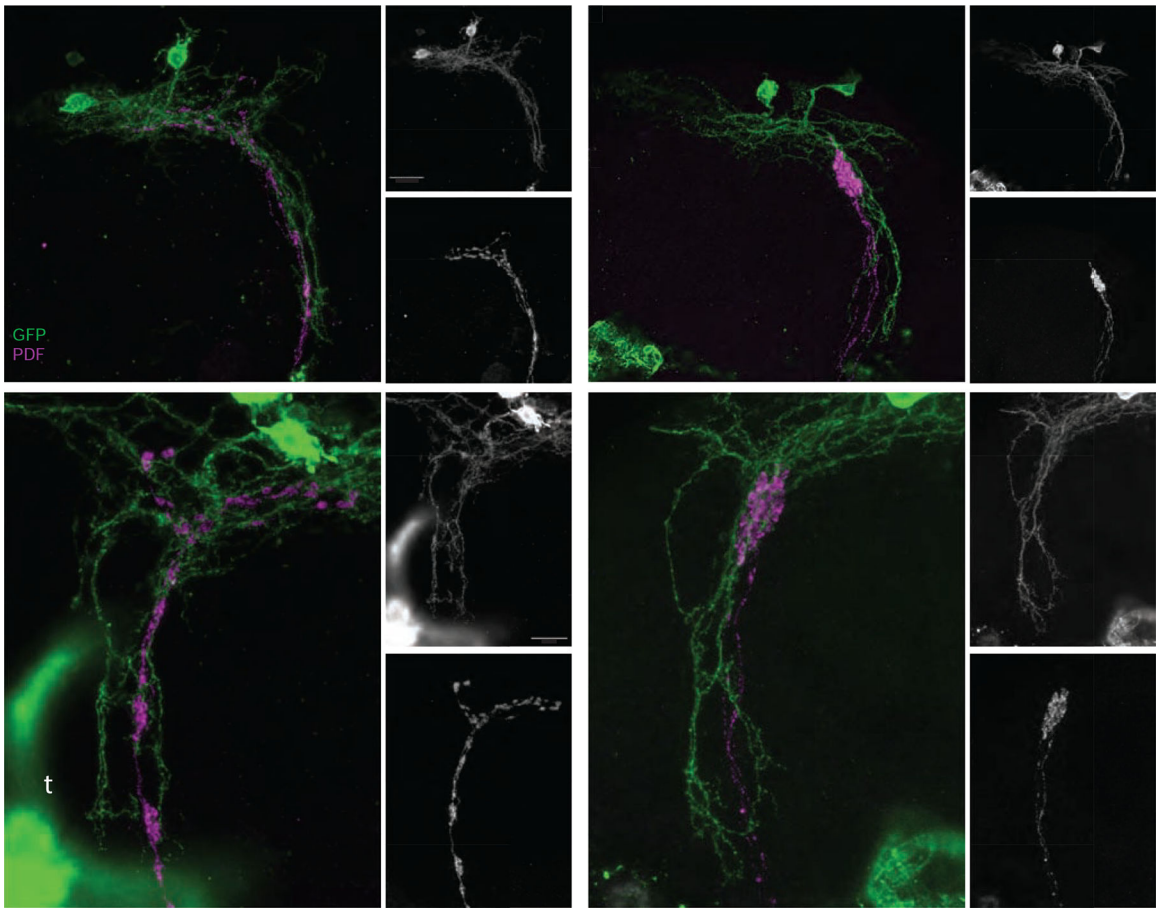

Figure 4. The expression of Unc5 causes significant changes in the anatomical relationship between the neurites of the DN1$_p$s and the dorsal projections of the s-LN$_v$s.

(**A-C**) Confocal reconstruction of s-LN$_v$ dorsal projections and the neurites of the DN1$_p$ clock neurons in the dorsal protocerebrum of a ;*Pdf-Gal4/LexAop-mCD8:GFP;Clk4.1LexA/+* brain. (**A**) Brains were immuno-labelled for GFP (green) and PDF (magenta) and imaged through the posterior surface of the brain. Small panels display single gray scale projections of GFP (**B**) and PDF expression (**C**). The medial (m), lateral (l) and ventral (v) extensions of the DN1$_p$ neurons are indicated in B and the medial (m) and lateral (l) extensions of the s-LN$_v$ dorsal termini are indicated in C. (**D-F**) Confocal reconstruction of s-LN$_v$ dorsal projections and the neurites of the DN1$_p$ clock neurons in the dorsal protocerebrum of a ;*Pdf-Gal4/LexAopmCD8:GFP;Clk4.1LexA/UAS-Unc5* brain immunolabeled and imaged as described for A-C. The major extensions of the DN1$_p$s are intact, yet the medial and lateral extensions of the s-LN$_v$s are completely absent. Merged GFP and PDF signals are shown in D. Small panels display single gray scale reconstructions of GFP (**E**, labels as for B) and PDF expression (**C**). (**G-H**) High magnification confocal reconstruction of the dorsal projections of normal s-LN$_v$s (magenta) and their relationship with the ventral projection of the DN1$_p$s. The genotype is the same as in A and panels organized and labeled as for A-C. High levels of GFP are expressed in the tracheae (t in panel G). (**J-L**) High magnification projection of an Unc5-expressing s-LN$_v$ dorsal projection and neighboring DN1$_p$ neurons. The organization of the DN1$_p$ ventral extension

is unchanged by the truncated s-LN_vs. Panels organized and labeled as for D-F. Scale bars = 25 μm for A-F and 15 μm for G-L.

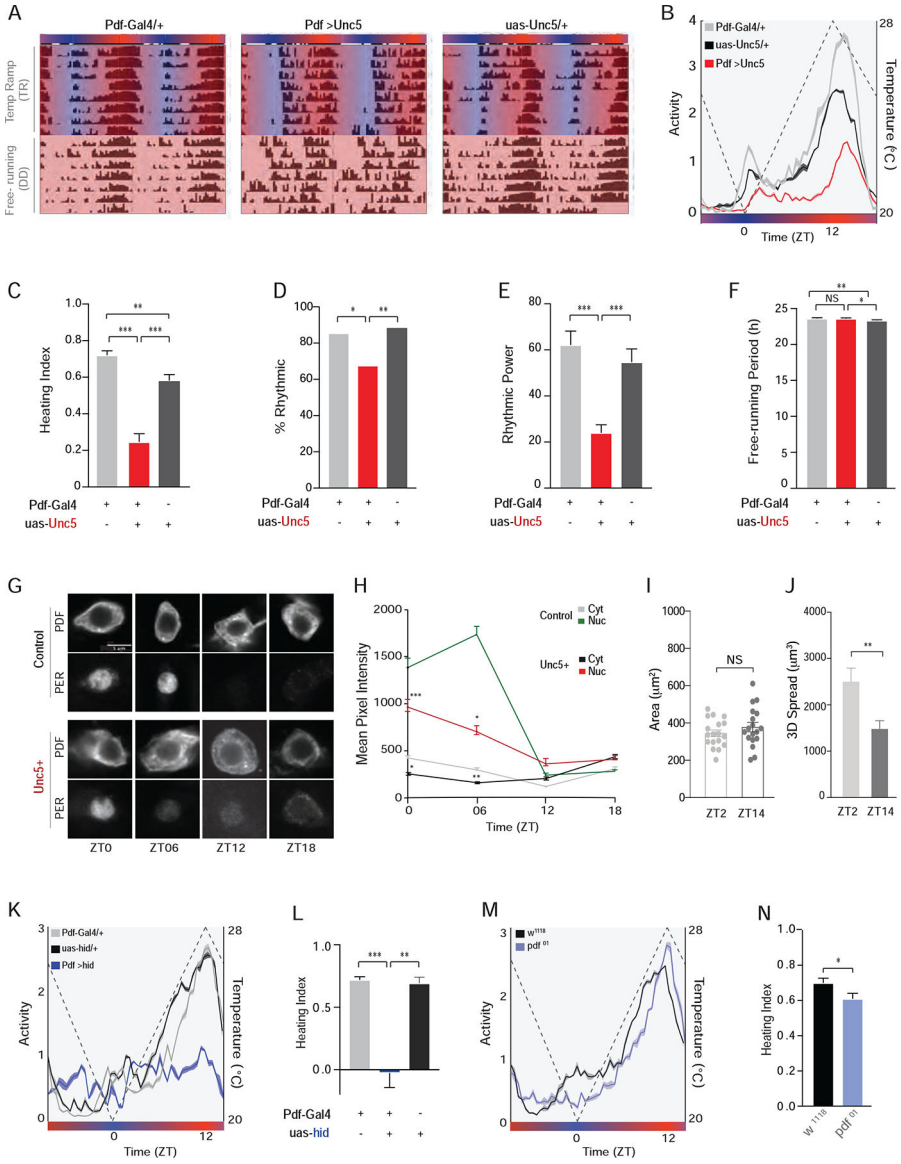

Figure 5. s-LN$_V$ terminal arbors mediate entrainment to temperature ramps.

(**A**) Representative actograms of single flies entrained for 8-days to constantly changing temperature ramps under DD followed by one week of free-run under DD at 25 °C. During entrainment, temperature progressively increased from 20 °C to 28 °C between ZT 0–12 (red shading) and gradually decreased from 28 °C to 20 °C between ZT 12–0 (blue shading). (**B**) Averaged population activity plots for the experimental *;PdfGal4/+;uas-Unc5/+* flies (red, N=32) and ;*Pdf-Gal4/+* (gray, N=32) and ;;*UAS-UNC5/+* (black, N=24) controls for the last three days of entrainment to the temperature cycle (days six to eight, indicated by white boxes in A). Dashed line represents temperature changes. (**C**) Heating indices, which reflect the correlation between heating and locomotor activity between ZT05 and 11 for the data shown in B. **(D)** Percentage of flies displaying significant circadian periodicity under constant 25 °C following temperature ramps. **(E)** Rhythmic power under constant 25 °C after temperature ramps. **(F)** Mean free-running period for seven days of constant 25 °C. **(G)**

Immunostaining of PER and PDF proteins in cells bodies of the s-LN_vs across the temperature cycle on day 5 of DD temperature ramp from control (top) and Unc5-expressing (bottom) s-LN_vs. Scale Bar = 5μm. **(H)** Quantification of nuclear and cytoplasmic PER immunosignals within the s-LN_vs. **(I)** Area (X-Y spread) of the dorsal projections is not significantly different between ZT 02 and 14 under temperature ramps. (**J**) Dorsal projections innervate larger brain volumes in the morning. (**K**)Averaged population activity plots and **(L)** heating indices for flies in which the proapoptotic gene *hid* was expressed in the PDF expressing LN_vs compared to heterozygote parental controls. **(M)** Averaged population activity plots and **(N)** heating indices for pdf^{01} mutants and their genetic background control, w^{1118}. See also Table S1 for statistical information and sample sizes and Figures S5–S7.

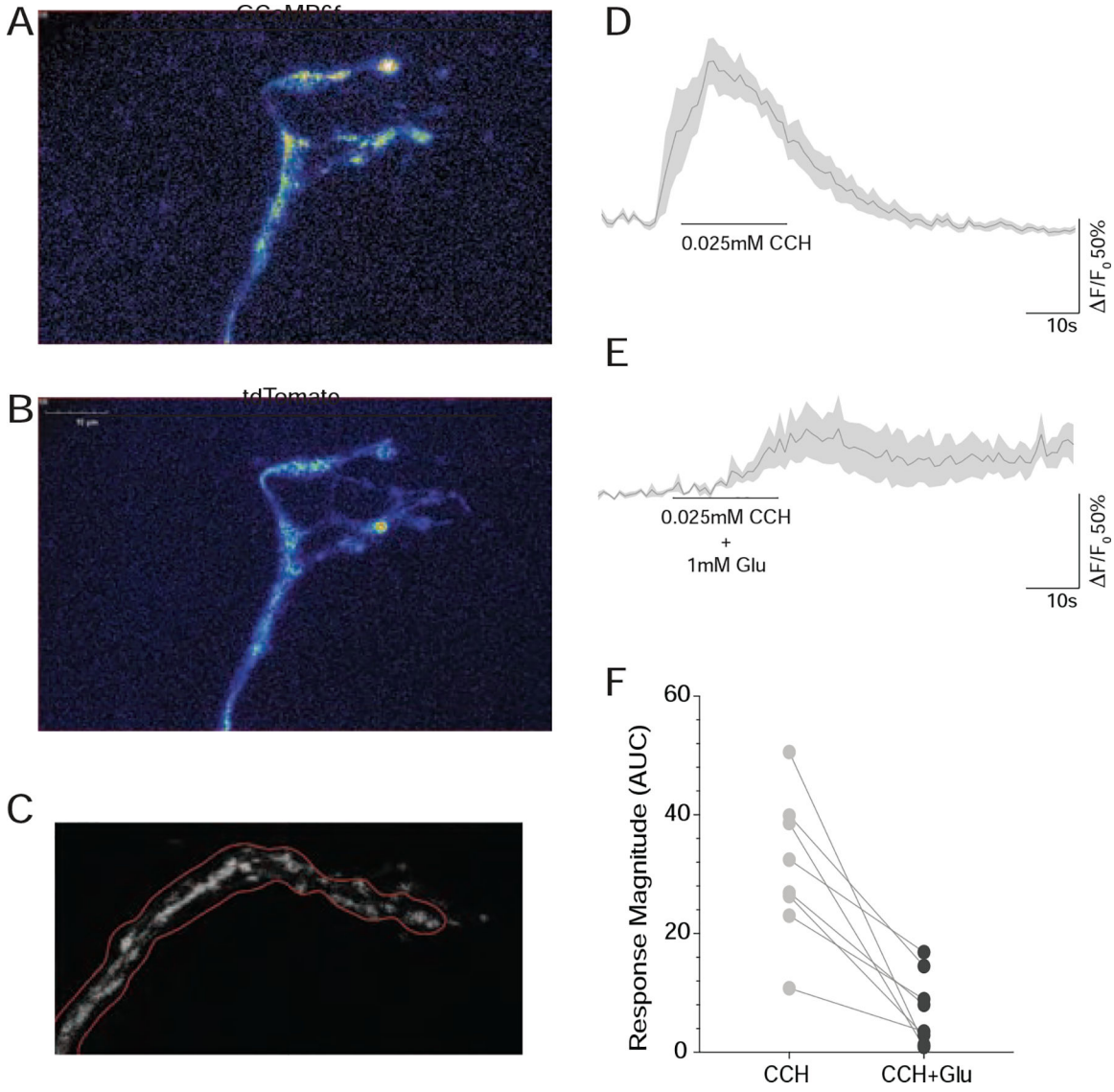

Figure 6. The terminal ramifications of the s-LNv dorsal projections are directly inhibited by bath applied glutamate.

(**A**) Rapid Z-series reconstruction of GCaMP6f expression in a living *Pdf(M)-Gal4/UAS-tdTomato/+;UAS-GCAMP6f/+* brain from the first timepoint of a representative volumetric timeseries of the s-LN_v dorsal termini. (**B**) the same brain volume scanned simultaneously for td-Tomato expression. (**C**) GCAMP6f fluorescence intensity was tracked in projected Z series over time with regions of interest that were automatically determined based on the pattern of tdTomato fluorescence. (**D**) Averaged GCAMP6f fluorescence traces from dorsal termini treated with 0.025mM Carbachol in the presence of of 2μM TTX. (**E**) Averaged GCAMP6f fluorescence traces from the same dorsal termini as in D, treated with 0.025mM Carbachol in the presence of 1mM glutamate in the presence of 2μM TTX. (**F**) Pairwise comparisons of the effects of CCh alone and CCh plus glutamate on eight s-LN_v dorsal termini. For every brain tested (n=8) glutamate reduced or abrogated the excitatory CCh response. Note that for all pairwise comparisons, CCh plus glutamate was tested first,

followed immediately by CCh alone. See also Table S1 for statistical information and sample sizes and Figure S7.

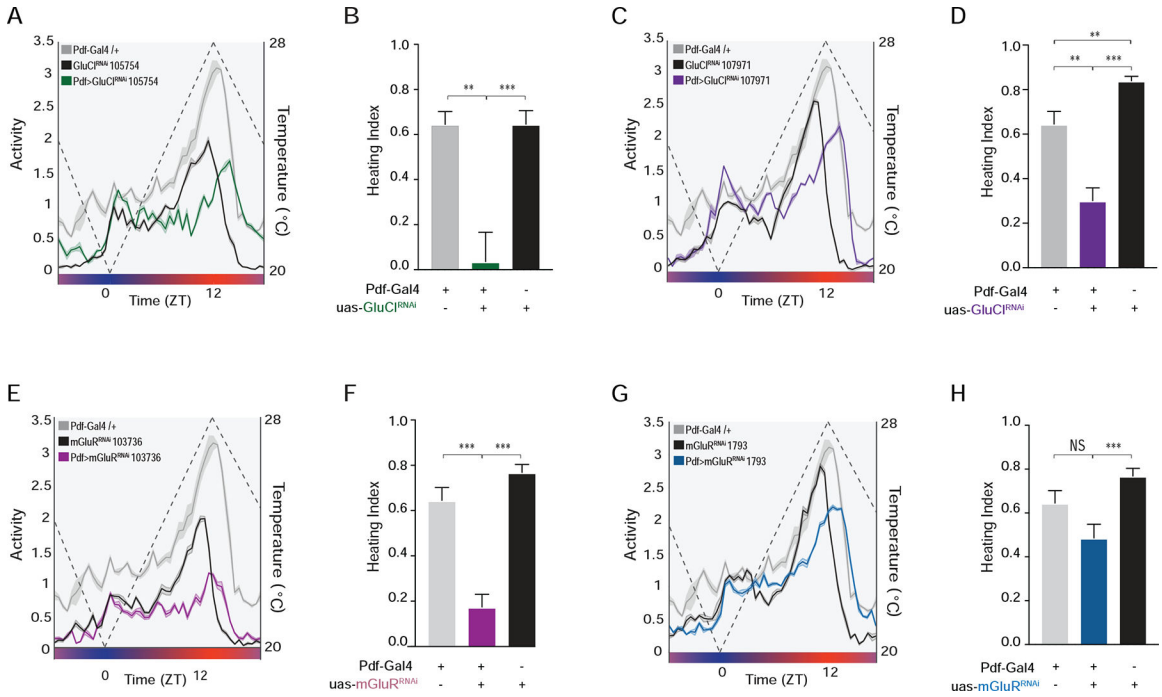

Figure 7. Knockdown of glutamate receptors in the LN_vs phenocopies the loss of their dorsal terminal arbors under temperature ramp cycles.

(A) Averaged population activity plots under ramping temperature cycles for experimental ;*Pdf-Gal4/UAS-GluCl-RNAi*; flies (green) and their parental heterozygous controls ;*Pdf-Gal4/+* (gray) and ;*UAS-GluCl-RNAi/+*; (black). Plots represent the last three days of entrainment to a ramping temperature cycle (days 6–8). The dashed line represents temperature changes. (**B**) Heating indices for the genotypes shown in A. **(C)** Averaged population activity plots for ;*Pdf-Gal4/UAS-GluCl-RNAi*; using a second RNAi construct and their parental controls. **(D)** Heating indices for the genotypes shown in C. **(E)** Averaged population activity plots for ;*Pdf-Gal4/UAS-mGluRRNAi*; and their parental controls. **(F)** Heating indices for the genotypes shown in E. **(G)** Averaged population activity plots for ;*Pdf-Gal4/+;UAS-mGluR-RNAi/+*; using a second RNAi construct and their parental controls. **(H)** Heating indices for the genotypes shown in G. For all histograms, * $P < 0.05$, ** $P < 0.01$, *** $P < 0.001$, and NS indicates not significantly different. For all activity plots, lines represent mean ± SEM. See Table S1 for statistical information and sample sizes.

KEY RESOURCES TABLE

REAGENT or RESOURCE	SOURCE	IDENTIFIER
Experimental Models: Organisms/Strains		
w;Pdf(BMRJ)-Gal4;	P. Taghert, Wash U Med. School	[15, 55]
w;;Pdf01	P. Taghert, Wash U Med. School	[15, 55]
yw;UAS-hid/CyO	P. Taghert, Wash U Med. School	RRID:BDSC_65403
w[1118];P(w[+mC]=Clk-lexA.4.1) 3/TM6C, Sb[1]	Amita Sehgal, U Penn	RRID:BDSC_80704
w;UAS-CD8:GFP;	Bloomington Stock left	RRID:BDSC_5130
w;;UAS-Dicer-2	Bloomington Stock left	RRID:BDSC_24651
yw;*Pdf-LexA*;	M. Rosbash, Brandeis	N/A
;*UAS-GluClα*^{RNAi};	Vienna *Drosophila* Resource left	ID 105754
w;*UAS-Fas2*;	*Dr. V. Budnik, UMaSS Med. School*	N/A
w;;UAS-Unc5-HA	*Barry Dickson, Janelia Farm*	[28]
UAS-Dscam-TM1-GFP; Pin/CyO;	Bing Ye, University of Michigan	[58]
;;UAS-Dbt^{LONG} *myc(27MIC)/(TM3)*	Jeffrey Price, University of Missouri at Kansas City	[59]
w;;20xUAS-GCamp6f	Bloomington Stock left	RRID:BDSC_52869
w;LexAop-mCD8GFP;TM2/TM6B,Tb	Bloomington Stock left	RRID:BDSC_66545
Uas-mGluR-RNAi;	Vienna Drosophila Resource left	ID 103736
;*UAS-GluClα*^{RNAi};	Vienna Drosophila Resource left	ID 107971
w;;UAS-mGluR-RNAi	Vienna Drosophila Resource left	ID 1793
Antibodies		
Mouse anti-PDF (1:500)	Developmental Hybridoma Bank	DSHB Cat# DPDF-P (nb33), RRID:AB_10805428
Guinea pig anti- PAP (1:500)	Paul Taghert Lab	N/A
Rabbit anti-GFP (1:1000)	Invitrogen A-6455	(Molecular Probes Cat# A-6455, RRID:AB_221570) Comments: Discontinued; This product offered by Molecular Probes (Invitrogen A-6455)
Software		
Fiji	http://fiji.sc	RRID: SCR_002285
Imaris	Bitplane	RRID:SCR_007370
Matlab R2018a	MathWorks	RRID: SCR_001622
GraphPad Prism 8.0	GraphPad Software	RRID: SCR_002798
R	The R Foundation	RRID:SCR_001905
DAM FileScan	Trikinetics	[65]
ClockLab	Actimetrics	RRID:SCR_014309
R package for Circular Statistics	Dr. Boyan Kostadinov, code developed for this study.	The code generated during this study is available at: https://github.com/bkostadi/circular_analysis
Chemicals, Peptides, and Recombinant Proteins		
HardSet Vectashield Mounting Medium	Vector Laboratories	RRID:AB_2336787

REAGENT or RESOURCE	**SOURCE**	**IDENTIFIER**
L-Glutamic Acid	Sigma-Aldrich	PubChem ID: 24895052
Carbachol Chloride (CCH)	Tocris, Bristol, U.K.	PubChem ID: 5831
Tetrodotoxin citrate (TTX)	Tocris, Bristol, U.K.	PubChem ID: 16759596
Premix PBS Buffer (10x)	Sigma-Aldrich	Cat# 11666789001
Triton X-100	Sigma-Aldrich	Cat#X100; CAS: 9002-93-1
Bacto Agar	Becton Dickinson Microbiology	Cat#214010
Sucrose	Sigma-Aldrich	Cat#S7903; CAS: 57-50-1
Other		
DAM2 *Drosophila* Activity Monitors	Trikinetics	[65]
DAM Drosophila Environmental Monitors	Trikinetics	[65]